Improved Evaluation of BBR and Collisional Frequency Shifts of NIM-Sr2 with 7.2×10^{-18} Total Uncertainty

Bing-Kun Lu(卢炳坤)[1,2], Zhen Sun(孙震)[1,2], Tao Yang(杨涛)[1], Yi-Ge Lin(林弋戈)[1*], Qiang Wang(王强)[1], Ye Li(李烨)[1], Fei Meng(孟飞)[1], Bai-Ke Lin(林百科)[1], Tian-Chu Li(李天初)[1], and Zhan-Jun Fang(方占军)[1*]

[1]*Division of Time and Frequency Metrology, National Institute of Metrology, Beijing 100029, China*
[2]*Department of Precision Instrument, Tsinghua University, Beijing 100084, China*

(Received 22 April 2022; accepted manuscript online 13 July 2022)

NIM-Sr2 optical lattice clock has been developed on the Changping campus of National Institute of Metrology (NIM). Considering the limitations in NIM-Sr1, several improved parts have been designed including a differential pumping stage in the vacuum system, a permanent magnet Zeeman slower, water-cooled anti-Helmholtz coils, an extended viewport for Zeeman slower, etc. A clock laser with a short-time stability better than 3×10^{-16} is realized based on a self-designed 30-cm-long ultra-low expansion cavity. The systematic frequency shift has been evaluated to an uncertainty of 7.2×10^{-18}, with the uncertainty of BBR shift and the collisional frequency shift being an order of magnitude lower than the last evaluation of NIM-Sr1.

DOI: 10.1088/0256-307X/39/8/080601

Optical clocks have realized better stability and smaller uncertainty compared with ^{133}Cs fountain clocks.[1–3] Potential applications of optical clocks include global navigation satellite systems,[4] geodesy measurement,[5] gravitational wave detection,[6] and dark matter searching,[7] etc. Up to date, 11 optical transitions have been defined as the secondary representations of the second by the International Committee for Weights and Measures (CIPM).[8] The strontium optical lattice clock, with its superior stability and uncertainty, is one of the most competitive candidates for the redefinition of the second in the future. NIM started the research of the strontium optical lattice clock (NIM-Sr1) in 2006. The first systematic shifts evaluation of NIM-Sr1, located on Hepingli campus, was carried out in 2015 with an uncertainty of 2.3×10^{-16},[9] mainly limited by its lattice AC Stark shift and black body radiation (BBR) shift. In 2020, after some major improvements,[10] NIM-Sr1 was evaluated with a systematic uncertainty of 2.9×10^{-17}.[11] In 2017, we started to build the second strontium optical lattice clock (NIM-Sr2) in our new Changping campus. In this Letter, we report the development of the NIM-Sr2 system and its systematic shifts evaluation.

Schematic of the vacuum system of NIM-Sr2 is shown in Fig. 1. The atomic beam is generated from the oven, which is heated to about 520 ℃. The atomic beam is collimated by a two-dimensional (2D) collimator, slowed down by a Zeeman slower, and captured at the MOT chamber. Compared to NIM-Sr1,[12] the main improvements of NIM-Sr2 include a differential pumping stage, a ring-shaped permanent magnet Zeeman slower, water tube constructed anti-Helmholtz coils, and the extended viewport for Zeeman slower.

A differential pumping stage is added between the oven and the magneto-optical trap (MOT) chamber. The differential pumping stage includes a small chamber that holds a mechanical shutter for shutting off the atomic beam, a differential tube with 90 mm in length and 6 mm in diameter that connects the 2D collimator, and a second differential tube that makes use of the Zeeman slower tube. Three ion pumps are connected to the 2D collimator, the differential pumping chamber, and the MOT chamber, respectively. Two vacuum gauges are used to monitor the vacuum pressure. After refilling the strontium oven, the vacuum pressures at the 2D collimator and the MOT chamber are 2.6×10^{-8} Pa and 2.0×10^{-7} Pa with the oven off, and 1.7×10^{-7} Pa and 2.1×10^{-7} Pa with the oven on. This shows that the differential pumping stage is very effective to keep the low vacuum pressure of the MOT chamber from the operation of the hot oven.

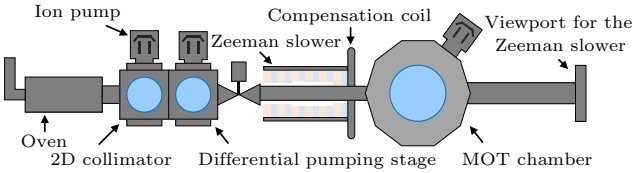

Fig. 1. Schematic of the NIM-Sr2 vacuum system.

The magnetic field of the Zeeman slower of NIM-Sr1 is generated by a double tapered multi-layer coil.[13] Although the Zeeman slower of NIM-Sr1 is water-cooled, considerable heat is still generated at the adjacent part of the MOT chamber when the Zeeman slower is turned on. In order to reduce the uncertainty of the BBR shift, the temperature homogeneity of the MOT region needs to

*Corresponding authors. Email: linyige@nim.ac.cn; zfang@nim.ac.cn
© 2022 Chinese Physical Society and IOP Publishing Ltd

be optimized. Zeeman slower is changed from an electric solenoid to longitudinal ring-shaped permanent magnets, which has neither power consumption nor vibration noise induced by the water-cooling system. The new Zeeman slower is composed of 40 permanent magnet rings with the same outer diameter but different inner diameters.[14] The maximum variation of the magnetic field from its designed value along the longitudinal axis is about 2%, and it is less than 1% fluctuation in the central 5 mm along the radial axis. Finally, about 2% of ^{87}Sr atoms are slowed down to less than 50 m/s, and loaded into the blue MOT. At the end of the Zeeman slower near the MOT chamber, a small coil is used to compensate for the gradient of the magnetic field at the center of the MOT chamber.

In the first stage of laser cooling, the magnetic field gradient required at the MOT center is about 50 G/cm, and the operating current of the anti-Helmholtz coils is about 50 A. The heat generated by the coils needs to be well managed to control the thermal environment of the atoms. Therefore, the anti-Helmholtz coils are made of hollow copper tubes with a 5 mm outer diameter and 3 mm inner diameter. The heat generated by the coils is taken away by the cooling water running through the hollow copper tubes. The tubes of the coils are sealed and bonded using epoxy. The winding of the coils is referenced to Ref. [15] to improve the temperature control of the MOT chamber.[16] To improve the temperature uniformity of the two coils, it is necessary to ensure that the flow and the temperature of the coolant in the two coils are the same. Therefore, the water inlets of the two coils are connected in parallel and two flow sensors are installed to monitor the flow rates. In case of an accidental chiller failure or insufficient cooling capacity, an alarm is generated and the coils will be shut down automatically.

The viewport for the Zeeman slowing laser beam is extended 30 cm away from the MOT chamber. This design reduces the solid angle of the hot port views by the atoms trapped at the MOT center, which helps to reduce the BBR shift. In addition, some atoms which are no sufficiently slowed down by Zeeman slower may deposit on the viewport of the Zeeman slower, which may block some of the Zeeman slowing laser beam. This extension also reduces the deposition.

The direction of the one-dimensional optical lattice of NIM-Sr2 is set to an angle of 12° with respect to the direction of gravity, which is different from the near-horizontal setup of NIM-Sr1.[12] The tunneling effect is effectively suppressed by the gravitational potential energy difference between lattice sites in this design.[17]

Based on this improved NIM-Sr2 experimental setup, the side-band resolved spectrum shows that the atoms' temperature in the lattice was cooled down to ∼2.6 μK along the longitudinal axis and ∼6.7 μK in the radial direction.[18] With an interrogation time of 200 ms and a scanning step of the clock laser frequency of 0.1 Hz, the obtained Rabi spectrum linewidth is about 4.2 Hz, as shown in Fig. 2(b). All the evaluation experiments involved in this study are carried out under this condition.

The uncertainty of the BBR shift is the dominant contribution to the overall systematic shifts uncertainty of optical clocks. The BBR generally comes from the MOT chamber and other ambient heat sources. The BBR shift is expressed as[19]

$$\Delta\nu_{\rm eg} = -\frac{\Delta\alpha_{\rm eg}(0)}{2\,h}\langle E^2(t)\rangle[1+\eta(t)], \tag{1}$$

where $\Delta\alpha_{\rm eg}(0)/h = 61.5558(17)\times10^{-7}\,{\rm Hz\cdot V^{-2}\cdot m^2}$ is the static differential polarizability between the ground state and the excited state, $\langle E^2(t)\rangle = [8.319430(15)\,{\rm V/cm}]^2(\frac{T}{300\,{\rm K}})^4$ is the mean square electric field, and $\eta = 0.06980(33)$ is the dynamic correction factor.

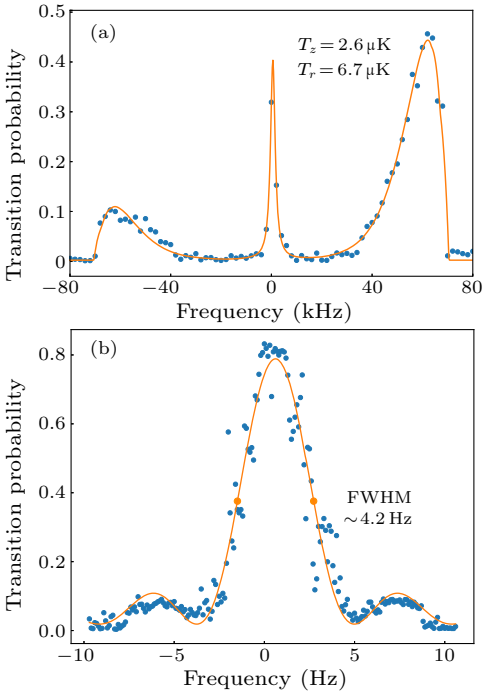

Fig. 2. (a) Sideband-resolved spectrum and (b) linewidth with a Rabi excitation pulse width of 200 ms.

Based on the earlier mentioned improvements including the Zeeman slower, the anti-Helmholtz coils and the extended viewport for Zeeman slower, an infrared thermal imager is used to help us to map the temperature gradient of the MOT chamber, which is important to arrange the positions of the temperature sensors. It is also important to adjust and optimize the temperature of the cooling water in the anti-Helmholtz coil carefully to make the temperature gradient around the atoms as small as possible. Considering the influence of ambient heat sources and the cooling water, four out of eight available sensors are mounted near the coils, one near the viewport of Zeeman slower, and two on different viewports, as indicated in Fig. 3. All of them are fixed to the MOT chamber with thermal conductive tapes. The last one samples the room temperature.

The effective temperature $T_{\rm eff}$ and its uncertainty u_T of the environment are used to evaluate the BBR shift. According to the common evaluation methods

when the complete thermal model of the environment is unknown,[16,19,20] a uniform or rectangular distribution model is used to evaluate the effective temperature $T_{\rm eff}$ and its uncertainty u_T. Assuming that the highest value of the ambient temperature of the atom is $T_{\rm max}$ and the lowest value is $T_{\rm min}$, the effective temperature of the black body $T_{\rm eff}$ and its uncertainty u_T can be expressed as

$$T_{\rm eff} = (T_{\rm max} + T_{\rm min})/2, \quad u_T = (T_{\rm max} - T_{\rm min})/\sqrt{12}. \quad (2)$$

As shown by Eqs. (1) and (2), the uncertainty of the BBR frequency shift is predominantly dependent on u_T, and u_T is dependent on the temperature inhomogeneity of the MOT chamber surrounding the trapped cold atoms. Therefore, for an accurate evaluation of the BBR frequency shift, it is very important to reduce the temperature gradient and to accurately measure the temperature extremes of the MOT chamber.

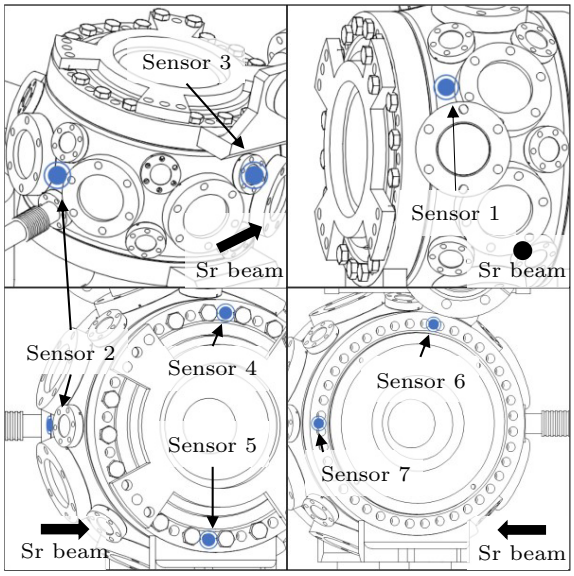

Fig. 3. Layout of the sensors on the MOT chamber.

In order to achieve a better evaluation uncertainty, an accurate calibration of the temperature measurement unit and sensors is necessary. In our experiment, a precision temperature scanner (Fluke, 1586 A) and high precision commercial platinum resistors (PT100-385) with four-wire configuration are used. The temperature scanner is equipped with a 10-channel multiplexer module (Fluke, 1589–2588). Under a slow scanning rate (4 s per channel), the temperature scanner has a measurement accuracy of ±5 mK for platinum resistance thermometers (PRTs). The default accuracy of these commercial class-A PRTs is 150 mK, which is not accurate enough for BBR shift evaluation. After the calibration of the scanner together with PRTs in analogy to real experimental conditions by the Division of Thermophysics Metrology of NIM,[11] the temperature measurement uncertainty is reduced to less than 7 mK in the range from 20 ℃ to 26 ℃, which corresponds to a BBR frequency shift uncertainty of $\sim 2 \times 10^{-18}$.

The periodic fluctuation of the temperature difference mainly follows the fluctuation of the room temperature, as shown in Fig. 4(a). The influence of ambient heat sources mentioned above is inevitable and this is the limitation of the temperature inhomogeneity. The maximum temperature difference between PRTs mounted on the MOT chamber is 0.166 K as shown in Fig. 4(b). Compared with NIM-Sr1, the maximum temperature difference is reduced by 80%, benefitting from the previously mentioned designs which help to reduce the temperature gradient. According to Eq. (2), $T_{\rm eff}$ is 297.07 K and u_T is 0.05 K, in which the measurement uncertainty is included. The BBR shift induced by the MOT chamber is -5105.1×10^{-18} with an uncertainty of 3.8×10^{-18}.

The procedure of evaluating the BBR shifts from the heated oven and the extended viewport for the Zeeman slower is the same as the previous evaluation of NIM-Sr1.[11] Based on the dimensions of the NIM-Sr2 system, the solid angle of the heated oven and the extended viewport for the Zeeman slower to atoms are 5.90×10^{-5} sr and 4.72×10^{-3} sr, respectively. With the oven's temperature of 793(50) K and the viewport's temperature of 353(20) K, the BBR frequency shift of these two parts is $-11.3(4.0) \times 10^{-18}$.

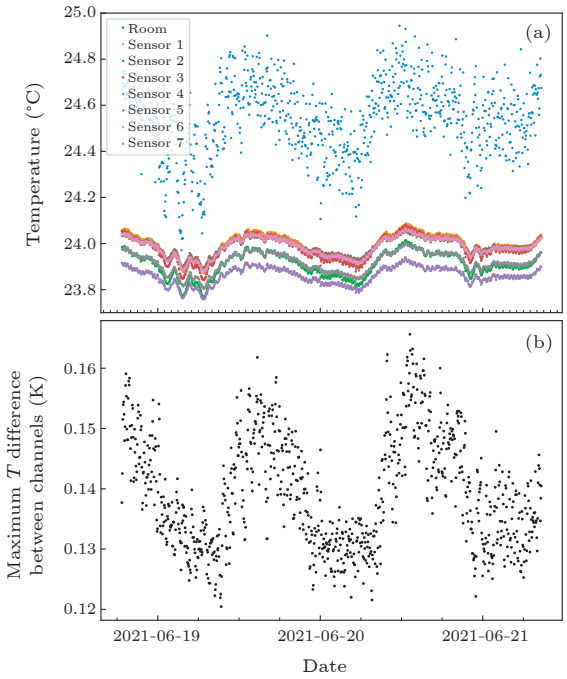

Fig. 4. (a) Temperature of 8 scanner channels and (b) the maximum temperature difference among 8 temperature scanner channels.

The uncertainty of the collisional shift is the second largest contribution to the total systematic frequency uncertainty in our strontium optical clocks.[9,11] To improve the measurement accuracy of the collisional shift, an ultrastable clock laser is developed for NIM-Sr2.

In the beginning, NIM-Sr2 uses a 10-cm-long ultra-low expansion (ULE) cavity C1 as the reference for the optical local oscillator (OLO).[21] It is necessary to improve the short-time stability of the OLO, typically by increasing the cavity length and changing the mirror substrates

to reduce the thermal noise influence.[10,22] We design a ULE cavity C2 with a 30-cm-long ULE spacer and a pair of high reflectivity fused silica mirrors. The average lifetime τ of photons in the cavity is about 66.8 µs measured by the ring-down spectroscopy technique, corresponding to a cavity finesse of about 210000.

The cavity is supported on a zerodur base with four fluorine rubber balls, whose positions have been optimized by the finite element analysis method aimed to minimize the sensitivity to the ambient vibration noise. As shown in Fig. 5, the whole vacuum chamber includes four layers. The outermost layer is an aluminum vacuum house, with a 75 L/s ion pump to keep the pressure at about 2.4×10^{-6} Pa. One active temperature control layer and two passive thermal shield layers are arranged in the vacuum house. Copper with high thermal conductivity is used for these three inner layers, while polyamide-imide (PAI) balls with low thermal conductivity are used between the layers to reduce the heat transfer between different layers. To reduce the heat exchange caused by radiation, the copper layers are polished and plated with gold to reduce the thermal emissivity. The vacuum chamber is placed on an active vibration isolation platform.

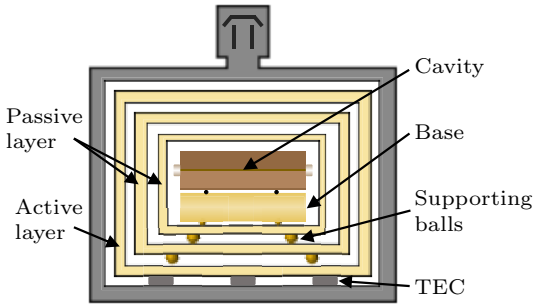

Fig. 5. A section structure diagram of the reference cavity.

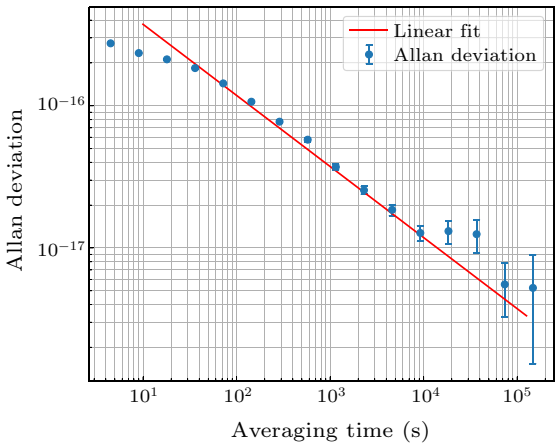

Fig. 6. Allan deviation of the collisional shift measurement with the time-interleaved self-comparison. The linear fit of interleaved instability, shown in the red solid line, is $1.18 \times 10^{-15}/\sqrt{\tau}$.

To ensure the continuity of the experiment and the reliability of the system, the optical layout of C2 is built based upon the original one, that is, the laser locked to C2 through an AOM is pre-stabilized to C1. With the above improvements, the robustness of the OLO is improved, and the laser can stay locked for several weeks. The Allan deviation from the collisional shift measurement with the time-interleaved self-comparison is shown in Fig. 6. The short term frequency stability of the OLO can be evaluated from it,[23] which is approximately 2.8×10^{-16} at 1 s, not far from the theoretical thermal noise limit of 1.4×10^{-16}.[24]

To evaluate the collisional shift, the density of the trapped cold atoms is modulated by modulating the loading time of the blue MOT with a factor of 2. Similar to NIM-Sr1, an energy filtering method is used to reduce the density of cold atoms and filter the relatively hot atoms out in the evaluation.[11] By expressing the density of the cold atoms as the voltage detected by the photomultiplier (PMT), the collisional shift coefficient is $a_{\text{density}} = -0.000627(99)$ Hz/V, based on a long measurement campaign with 1000 valid data as a set of packets shown in Fig. 7. The distribution of the density measurement data sets does not fit a perfect normal distribution, so it is appropriate to introduce a chi-squared correction to the uncertainty.[25] The correction of the collisional frequency shift is $58.5(3.1) \times 10^{-18}$, and its uncertainty is reduced by one order of magnitude compared with NIM-Sr1.

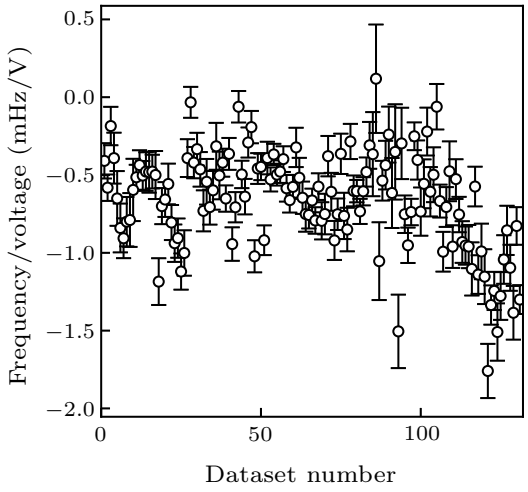

Fig. 7. Coefficient measurement of the collisional shift.

The frequency of the lattice laser at 813 nm is locked to a 10-cm-long reference cavity at about 368554.41 GHz. The intensity of the lattice laser is modulated to measure the frequency difference when atoms are at different trap depths. A laser power stabilization unit is established to actively control different lattice trap depths synchronized with the operating time sequence of NIM-Sr2. When the trap depth is modulated, the density of the lattice trapped atoms is also changed. The collisional shift caused by the trap depth modulation is corrected in the measurements, using the density shift coefficient measured in the previous experiment. According to Ref. [26], the coefficients of E1 polarizabilities, M1/E2 polarizabilities and hyperpolarizabilities have been accurately measured and adopted by other groups,[27,28] despite their

consistency with the former theoretical and experimental results. With the lattice depth of $114E_r$ (E_r is the photon recoil energy) and the mean vibrational state occupation of 0.34, the scalar/tensor light shift is estimated to be $-11.5(2.6) \times 10^{-18}$. The frequency shifts of the hyperpolarizability and M1/E2 are $11.9(0.4)\times10^{-18}$ and $20.1(0.8) \times 10^{-18}$, respectively.

The Zeeman effect caused by the biased magnetic field also shifts the transition frequency. During the locking process, $m_F = +9/2$ and $m_F = -9/2$ components of the clock transition are locked and their average is taken as the transition frequency to eliminate the first-order Zeeman shift. NIM-Sr2 has a better spectral resolution than NIM-Sr1, and NIM-Sr2 supports to use a smaller bias magnetic field to reduce the uncertainty of second-order Zeeman shift. The second-order Zeeman shift is $-105.2(0.1) \times 10^{-18}$ with a bias magnetic field to set the frequency difference between the two components to be 428.726(3) Hz and the coefficient given in Ref. [17].

The stray electric field especially caused by the electrostatic charge trapped in the MOT chamber viewport coatings will introduce a DC Stark shift.[29] With the same method used in evaluating the DC Stark shift in NIM-Sr1,[11] after treating the MOT viewports with UV lights, the DC Stark shift is measured to be $-20.9(0.2) \times 10^{-18}$ by alternating DC voltages between two indium tin oxide (ITO) coated transparent electrode around the atoms.

Collisional induced frequency shift due to background gas is also needed to be considered.[30] The lattice lifetime is measured to be 3.0(0.1) s,[31] and the background gas collisional shift is evaluated to be $-10.0(1.1) \times 10^{-18}$. With a Rabi interrogation time of 200 ms, the intensity of the clock laser is only a few nanowatts. The probe beam AC Stark shift is less than 1×10^{-18},[27,32] which is totally used as the uncertainty. The energy filtering process and a nearly vertical lattice help to reduce the influence of the tunneling effect.[16] Similar to NIM-Sr1, a second integration is also introduced to reduce the servo error.[11] Tunneling and servo error are evaluated less than 1×10^{-18}. The relative systematic frequency shifts and uncertainties of NIM-Sr2 are listed in Table 1.

Table 1. Relative systematic frequency shifts and uncertainties of NIM-Sr2.

Systematic effect	Correction (10^{-18})	Uncertainty (10^{-18})
BBR MOT Chamber	5105.1	3.8
BBR oven and viewport of Zeeman	11.3	4.0
Lattice scalar/tensor	11.5	2.6
Lattice hyperpolarizability	−11.9	0.4
Lattice M1/E2	−20.1	0.8
Collisions	58.5	3.1
Second Zeeman	105.2	0.1
Background gas collisions	10.0	1.1
DC Stark	20.9	0.2
Probe AC stark	0.0	1.0
Servo error	0.0	1.0
Tunneling	0.0	1.0
Total	5290.5	7.2

In summary, we have developed the NIM-Sr2 strontium optical lattice clock on Changping campus with a systematic frequency shift uncertainty of 7.2×10^{-18}, by making improvements on the BBR and collisional shifts evaluation compared to NIM-Sr1. The BBR shift still contributes the largest uncertainty. Modeling the temperature gradient based on finite element simulation and putting thermometers inside the MOT chamber[33] are expected to map a more accurate temperature distribution around the atoms. A BBR shield is also considered to further reduce the uncertainty of BBR shift.[34] We plan to improve the evaluation of the BBR shift in the future.

Acknowledgments. This work was supported by the National Key R&D Program of China (Grant Nos. 2021YFF0603802 and 2016YFF0200201).

References

[1] Ushijima I, Takamoto M, Das M, Ohkubo T and Katori H 2015 *Nat. Photon.* **9** 185

[2] Huntemann N, Sanner C, Lipphardt B, Tamm C and Peik E 2016 *Phys. Rev. Lett.* **116** 063001

[3] Chou C, Hume D, Koelemeij J, Wineland D and Rosenband T 2010 *Phys. Rev. Lett.* **104** 070802

[4] Deschênes J D, Sinclair L C, Giorgetta F R, Swann W C, Baumann E, Bergeron H, Cermak M, Coddington I and Newbury N R 2016 *Phys. Rev. X* **6** 021016

[5] McGrew W F, Zhang X, Fasano R J *et al.* 2018 *Nature* **564** 87

[6] Kolkowitz S, Pikovski I, Langellier N, Lukin M D, Walsworth R L and Ye J 2016 Phys. Rev. D **94** 124043

[7] Derevianko A and Pospelov M 2014 *Nat. Phys.* **10** 933

[8] Riehle F, Gill P, Arias F and Robertsson L 2018 *Metrologia* **55** 188

[9] Lin Y G, Wang Q, Li Y, Meng F, Lin B K, Zang E J, Sun Z, Fang F, Li T C and Fang Z J 2015 *Chin. Phys. Lett.* **32** 090601

[10] Li Y, Lin Y, Wang Q, Yang T, Sun Z, Zang E and Fang Z 2018 *Chin. Opt. Lett.* **16** 051402

[11] Lin Y G, Wang Q, Meng F *et al.* 2021 *Metrologia* **58** 035010

[12] Lin Y G, Wang Q, Li Y *et al.* 2013 *Chin. Phys. Lett.* **30** 014206

[13] Shaokai W, Yuanyang Z, Baike L, Minming W and Zhanjun F 2008 *Conference on Precision Electromagnetic Measurements Digest*, 8–13 June 2008, Broomfield, CO, p 316

[14] Wang Q, Lin Y G, Gao F L, Li Y, Lin B K, Meng F, Zang E J, Li T C and Fang Z J 2015 *Chin. Phys. Lett.* **32** 100701

[15] Koller S B, Grotti J, Vogt S, Al-Masoudi A, Dörscher S, Häfner S, Sterr U and Lisdat C 2017 *Phys. Rev. Lett.* **118** 073601

[16] Falke S, Lemke N, Grebing C *et al.* 2014 *New J. Phys.* **16** 073023

[17] Bothwell T, Kedar D, Oelker E, Robinson J M, Bromley S L, Tew W L, Ye J and Kennedy C J 2019 *Metrologia* **56** 065004

[18] Blatt S, Thomsen J W, Campbell G K, Ludlow A D, Swallows M D, Martin M J, Boyd M M and Ye J 2009 *Phys. Rev. A* **80** 052703

[19] Abdel-Hafiz M, Ablewski P, Al-Masoudi A *et al.* 2019 arXiv:1906.11495 [physics]

[20] BIPM 2008 JCGM 100:2008(E), Evaluation of measurement data—Guide to the expression of uncertainty in measurement, produced by Working Group 1 of the Joint Committee for Guides in Metrology (JCGM/WG 1)

[21] Li Y, Lin Y G, Wang Q *et al.* 2014 *Chin. Phys. Lett.* **31** 024207

[22] Numata K, Kemery A and Camp J 2004 *Phys. Rev. Lett.* **93** 250602

[23] Peik E, Schneider T and Tamm C 2006 *J. Phys. B* **39** 145

[24] Notcutt M, Ma L S, Ludlow A D, Foreman S M, Ye J and Hall J L 2006 *Phys. Rev. A* **73** 031804

[25] Swallows M D, Bishof M, Lin Y, Blatt S, Martin M J, Rey A M and Ye J 2011 *Science* **331** 1043

[26] Ushijima I, Takamoto M and Katori H 2018 *Phys. Rev. Lett.* **121** 263202

[27] Hobson R, Bowden W, Vianello A, Silva A, Baynham C F A, Margolis H S, Baird P E G, Gill P and Hill I R 2020 *Metrologia* **57** 065026

[28] Hisai Y, Akamatsu D, Kobayashi T, Hosaka K, Inaba H, Hong F L and Yasuda M 2021 *Metrologia* **58** 015008

[29] Lodewyck J, Zawada M, Lorini L, Gurov M, and Lemonde P 2012 *IEEE Trans. Ultrason. Ferroelectr. Freq. Control* **59** 411

[30] Alves B X R, Foucault Y, Vallet G and Lodewyck J, 2019 *Joint Conference of the IEEE International Frequency Control Symposium and European Frequency and Time Forum (EFTF/IFC)*, 14–18 April 2019, Orlando, FL, USA, p 1

[31] Yasuda M and Katori H 2004 *Phys. Rev. Lett.* **92** 153004

[32] Hill I R and London I C 2012 *Development of an Apparatus for a Strontium Optical Lattice Optical Frequency Standard*, PhD Dissertation (London: Imperial College London)

[33] Nicholson T L *et al.* 2015 *Nat. Commun.* **6** 6896

[34] Beloy K, Hinkley N, Phillips N B, Sherman J A, Schioppo M, Lehman J, Feldman A, Hanssen L M, Oates C W and Ludlow A D 2014 *Phys. Rev. Lett.* **113** 260801